TELKOMNIKA Indonesian Journal of Electrical Engineering
Vol.12, No.7, July 2014, pp. 4988 ~ 4995
DOI: 10.11591/telkomnika.v12i7.4323

Electromagnetic-thermal Scale Model of Gas-Insulated Bus Bars

Li Hongtao*, Shu Naiqiu, Li Ling, Peng Hui, Li Zipin
School of Electrical Engineering, Wuhan University,
No.8, Donghunan Road, Hongshan District, Wuhan 430072, China
*Corresponding author, e-mail: 5pro@163.com

Abstract

Knowledge of the heat dissipation ability of gas-insulated bus bars (GIB) is paramount in the design stage. To reduce the capital cost, a scale model which has the identical electromagnetic-thermal characteristics of a full scale GIB is designed in this paper. The scaling relationships of the power losses, convection heat transfer, radiant heat transfer and thermal equilibrium are analyzed based on the governing equations and non-dimensional correlations. Current densities, power losses, convective heat transfer coefficients and temperature distributions in conductor and tank of the prototype and the scale models under different load currents are compared by FEM (Finite Element Method). The effectiveness of scale models is validated by the comparison between calculated and test results.

Keywords*: scale model, gas-insulated bus bars (GIB), temperature rise test, non-dimensional correlations, finite element method (FEM)*

1. Introduction

The current-carrying capacity is of critical importance to the design of gas-insulated bus bars (GIB), which is determined by the maximum permissible temperature [1]. The heat generation and dissipation in GIB, including power losses, convection and radiation, are complex problems. Therefore, investigation on electromagnetic-thermal characteristics of GIB is necessary in understanding the improvement of design and manufacture processes [2, 3].

Temperature rise test is the most direct and convincible means in investigating the electromagnetic-thermal characteristics of GIB. Tests have been carried out to analyze the temperature rise characteristics of the GIB [4]. Long term test of buried GIB is presented in [5]. However, the tests using full scale GIB are deemed to be costly and time consuming. Consequently, scale models, which have the advantages of good practicability and economy, have been widely employed to simulate the performance of many apparatus [6-8]. However, the scaling methods of multi-physical field problems cannot be realized by traditional linear scaling method, which are proved to be challenging tasks. Circuital and kinematic scaling relationships of the rail gun system, which is an electromagnetic-mechanical problem, are investigated and verified by numerical simulation [9]. The literature [10] has carried out a ground simulation test to study the thermal problem of spacecrafts under the condition of microgravity based on a fluid-thermal scale model and heat flow compensation technique.

In this paper, scaling method of electromagnetic-thermal problem in GIB is investigated. The scaling relationships of power losses and radiant heat transfer are derived from the governing equations, while the scaling of convection heat transfer is analyzed with the help of non-dimensional correlations. 1/4-scale models of the single- and three-phase GIB are established. The finite element method (FEM) is used to solve the coupled electromagnetic-fluid-thermal problem in GIB. The calculated results of the scale models are compared with those of the prototypes and the experimental data.

2. Scaling method

GIB is mainly composed of aluminum enclosure, conductor, epoxy resin insulators and insulating gas (SF_6). The cross sections of single- and three-phase GIB are shown, respectively, in Figure 1(a) and Figure 1(b). In the thermal analysis of GIB, the heat transfer mechanisms are

Received September 4, 2013; Revised February 5, 2014; Accepted March 7, 2014

conduction, convection and radiation. The heat generated in the conductor and the enclosure is transferred from the interior surface to the external surface by conduction. Natural convective heat transfer, which is caused by the density difference of the fluid, exists at the interface of the SF_6 gas and the conductor and that of the SF_6 gas and the enclosure. Thermal radiation heat transfer from the enclosure surface to the surrounding air and between the conductor and the enclosure is significant, especially when the temperature difference increases. To the authors' knowledge, approximately 60% of the heat generated in the GIB is dissipated to the surrounding air by radiation.

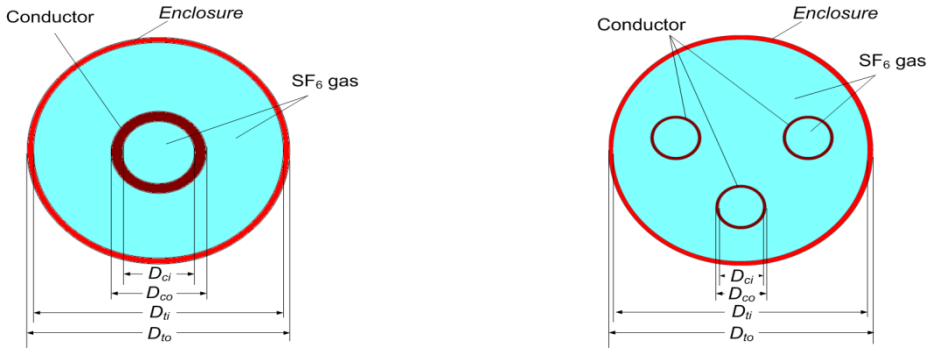

(a) Single-phase GIB (b) Three-phase GIB

Figure 1. Schematic Diagram of Single-phase and Three-phase GIB

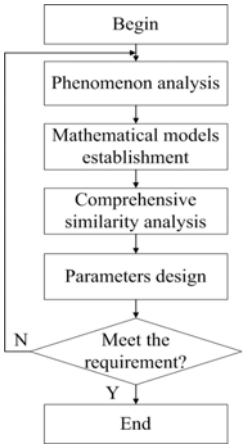

Figure 2. Flow Chart of Scaling on GIB

The flow chart of scaling on GIB is shown in Figure 2. First of all, the temperature rise mechanism of GIB is analyzed to build the mathematical models; secondly, derive the coupled field scaling relationships by analyzing the similarity of temperature rise in GIB theoretically; thirdly, discuss the parameters of scale model according to the scaling relationships; finally, assess the correctness and robustness of scale model by FEM and test results, if the scale model cannot satisfy the experimental requirements, the parameters should be further modified.

3. Similarity Analysis

3.1. Similarity of Power Losses

The following assumptions are made in the analysis process: displacement current is neglected; the current flowing in the conductor is sinusoidal; the reluctivity is considered as constant. $\boldsymbol{A}$, ϕ–$\boldsymbol{A}$ method is employed to investigate the eddy current problem, and the eddy

current field is divided into eddy current V_1 and non-eddy current region V_2. Governing equations of the two regions are described as [11]:

$$\begin{cases} \nabla\times(\nu\nabla\times\boldsymbol{A})-\nabla(\nu\nabla\cdot\boldsymbol{A})=\boldsymbol{J}_{\mathrm{e}}=-\sigma(T)\dfrac{\partial\boldsymbol{A}}{\partial t}-\sigma(T)\nabla\phi \\ \nabla\cdot(-\sigma(T)\dfrac{\partial\boldsymbol{A}}{\partial t}-\sigma(T)\nabla\phi)=0 \end{cases} \quad \text{in } \mathrm{V}_1 \tag{1}$$

$$\nabla\times(\nu\nabla\times\boldsymbol{A})-\nabla(\nu\nabla\cdot\boldsymbol{A})=\boldsymbol{J}_{\mathrm{s}} \quad \text{in } \mathrm{V}_2 \tag{2}$$

Where ν is the reluctivity, $\boldsymbol{A}$ is the magnetic vector potential, σ is the conductivity, t is the time, Φ is the electric scalar potential, $\boldsymbol{J}_{\mathrm{e}}$ and $\boldsymbol{J}_{\mathrm{s}}$ are, respectively, the eddy current density and source current density, T is the temperature.

Joule heat loss P_{c} in the conductor and eddy current loss P_{t} in the enclosure are expressed as:

$$P_{\mathrm{c}}=\frac{1}{2}\int_{\mathrm{V}}\frac{\left|\dot{\boldsymbol{J}}_{\mathrm{s}}\right|^2}{\sigma(T)}dv \tag{3}$$

$$P_{\mathrm{t}}=\frac{1}{2}\int_{\mathrm{V}}\frac{\left|\dot{\boldsymbol{J}}_{\mathrm{e}}\right|^2}{\sigma(T)}dv \tag{4}$$

According to the equations mentioned above, the similarity criterions of the power losses are summarized as:

$$\begin{cases} \dfrac{\sigma l^2}{\nu t}=\Pi_1,\dfrac{\sigma l\phi}{\nu A}=\Pi_2,\dfrac{J_{\mathrm{s}}l^2}{\nu A}=\Pi_3, \\ \dfrac{\nu^2A^2}{\sigma l^2P_{\mathrm{t}}}=\Pi_4,\dfrac{J_{\mathrm{s}}^2l^2}{\sigma P_{\mathrm{c}}}=\Pi_5 \end{cases} \tag{5}$$

3.2. Similarity of Heat Transfer

The traditional scaling of natural convection is based on the continuity equation, the Navier-Stokes equation and the energy equation. However, it is known that scaling relationships of natural convection heat transfer can hardly be fulfilled in multi-physical field problem because it is difficult to find out an appropriate fluid media. Because the temperature gradient on the outer surface of conductor and enclosure is not obvious, the scaling of average temperature on conductor and enclosure is fulfilled approximately by analyzing the rate of heat transfer, while the exact distribution of the convective heat transfer coefficient is not quite necessary. With regard to single-phase GIB, the equivalent thermal conductivity λ_{e} is used to calculate the convection heat transfer Q_{scc} between the conductor and the enclosure in (6) [4], and the radiant heat transfer Q_{scr} between the conductor and the enclosure is expressed in (7).

$$\begin{cases} Q_{\mathrm{scc}}=\dfrac{2\pi\lambda_{\mathrm{e}}\left(T_{\mathrm{c}}\text{-}T_{\mathrm{e}}\right)}{\ln\left(D_{\mathrm{ei}}/D_{\mathrm{co}}\right)} \\ \lambda_{\mathrm{e}}=\mathrm{C}_1\lambda_{\mathrm{f}}\left(\mathrm{Gr}\cdot\mathrm{Pr}\right)^{0.2}=\mathrm{C}_1\lambda_{\mathrm{f}}\left(\dfrac{g\alpha_{\mathrm{v}}\left(T_{\mathrm{c}}\text{-}T_{\mathrm{f}}\right)\left(D_{\mathrm{ei}}\text{-}D_{\mathrm{co}}\right)^3\rho_{\mathrm{f}}{}^2C_{\mathrm{p}}}{\mu_{\mathrm{f}}\lambda_{\mathrm{f}}}\right)^{0.2} \end{cases} \tag{6}$$

$$Q_{\mathrm{scr}}=\pi D_{\mathrm{co}}\delta\frac{\left(T_{\mathrm{c}}^{4}-T_{\mathrm{e}}^{4}\right)}{\frac{1}{\varepsilon_{\mathrm{co}}}+\frac{D_{\mathrm{co}}}{D_{\mathrm{ei}}}\left(\frac{1}{\varepsilon_{\mathrm{ei}}}-1\right)} \tag{7}$$

Where Gr_1 and Pr_1 are the Grashof number and the Prandtl number of SF_6, C_1 is a constant, D_{ei} and D_{co} are the inner diameter of enclosure and outer diameter of conductor respectively, T_c, T_e and T_f are the temperature of conductor, enclosure and SF_6, respectively. g is the gravity acceleration, ρ_f, C_p, λ_f and μ_f are, respectively, the density, specific heat, thermal conductivity and dynamic viscosity of SF_6, δ is Stefan-Boltzmann constant, ε_{co} and ε_{ei} are the emissivity of outer surface of conductor and inner surface of enclosure.

For three-phase GIB, the convection heat transfer Q_{tcc} and radiant heat transfer Q_{tcr} are expressed as [12]:

$$Q_{\mathrm{tcc}}=\frac{3\mathrm{C}_2 p^{0.6}D_{\mathrm{co}}^{0.75}\left(T_{\mathrm{c}}-T_{\mathrm{e}}\right)^{1.25}}{\left(2.2+\ln\frac{D_{\mathrm{ei}}}{2.4D_{\mathrm{co}}}\right)\left(1+2.4\left(\frac{D_{\mathrm{co}}}{D_{\mathrm{ei}}}\right)^{0.6}\right)^{1.25}} \tag{8}$$

$$Q_{\mathrm{tcr}}=3\pi D_{\mathrm{co}}\delta\frac{\left(T_{\mathrm{c}}^{4}-T_{\mathrm{e}}^{4}\right)}{\frac{1}{\varepsilon_{\mathrm{co}}}+\frac{D_{\mathrm{co}}}{D_{\mathrm{ei}}}\left(\frac{1}{\varepsilon_{\mathrm{ei}}}-1\right)} \tag{9}$$

Where p is the pressure of SF_6.

Q_{ec} and Q_{er} are the natural convection heat transfer and radiant heat transfer between the enclosure and the ambient air, which are described as:

$$\begin{cases}Q_{\mathrm{ec}}=\pi D_{\mathrm{eo}}h\left(T_{\mathrm{e}}-T_{\mathrm{a}}\right)\\ h=\dfrac{\lambda_{\mathrm{a}}\mathrm{C}_2\left(\mathrm{Gr}_2\cdot\mathrm{Pr}_2\right)^{0.3}}{D_{\mathrm{eo}}}=\dfrac{\lambda_{\mathrm{a}}\mathrm{C}_2}{D_{\mathrm{eo}}}\left(\dfrac{g\alpha_{\mathrm{v}}\left(T_{\mathrm{e}}-T_{\mathrm{a}}\right)D_{\mathrm{eo}}{}^{3}\rho_{\mathrm{a}}{}^{2}C_{\mathrm{pa}}}{\mu_{\mathrm{a}}\lambda_{\mathrm{a}}}\right)^{0.3}\end{cases} \tag{10}$$

$$Q_{\mathrm{er}}=\pi D_{\mathrm{eo}}\delta\varepsilon_{\mathrm{eo}}\left(T_{\mathrm{e}}^{4}-T_{\mathrm{a}}^{4}\right) \tag{11}$$

Where h is the convective heat transfer coefficient, T_a is the ambient temperature, Gr_2 and Pr_2 are the Grashof number and Prandtl number of ambient air, C_2 is a constant, D_{eo} is the outer diameter of enclosure, ρ_a, C_{pa}, λ_a and μ_a are, respectively, the density, specific heat, thermal conductivity and dynamic viscosity of air.

Heat transfer on the conductor and enclosure surfaces in steady state follows the thermal equilibrium equations.

$$\begin{cases}P_{\mathrm{c}}=\begin{cases}Q_{\mathrm{scc}}+Q_{\mathrm{scr}} & \text{single-phase case}\\ Q_{\mathrm{tcc}}+Q_{\mathrm{tcr}} & \text{three-phase case}\end{cases}\\ P_{\mathrm{c}}+P_{\mathrm{t}}=Q_{\mathrm{ec}}+Q_{\mathrm{er}}\end{cases} \tag{12}$$

The similarity indexes of convective heat transfer are summarized as follows:

$$\begin{cases} \dfrac{\lambda_{\mathrm{f}}^{0.8} l^{0.6} \rho_{\mathrm{f}}^{0.4} C_{\mathrm{p}}^{0.2}}{\mu_{\mathrm{f}}^{0.2} Q_{\mathrm{scc}}} = \Pi_6, \dfrac{p^{0.6} l^{0.75}}{Q_{\mathrm{tcc}}} = \Pi_7, \dfrac{l^{0.9}}{Q_{\mathrm{ec}}} = \Pi_8, \\ \dfrac{Q_{\mathrm{scr}}}{l\varepsilon_{\mathrm{co}}} = \Pi_9, \dfrac{Q_{\mathrm{tcr}}}{l\varepsilon_{\mathrm{co}}} = \Pi_{10}, \dfrac{Q_{\mathrm{er}}}{l\varepsilon_{\mathrm{eo}}} = \Pi_{11}, \dfrac{P_{\mathrm{c}}}{P_t} = \Pi_{12}, \\ \dfrac{P_{\mathrm{c}}}{Q_{\mathrm{scc}}} = \Pi_{13}, \dfrac{P_{\mathrm{c}}}{Q_{\mathrm{scr}}} = \Pi_{14}, \dfrac{P_{\mathrm{c}}}{Q_{\mathrm{tcc}}} = \Pi_{15}, \dfrac{P_{\mathrm{c}}}{Q_{\mathrm{er}}} = \Pi_{16}, \dfrac{P_{\mathrm{c}}}{Q_{\mathrm{ec}}} = \Pi_{17} \end{cases} \quad (13)$$

3. Scale Model Design

Using the same material, all the scale factors of the material parameters are set to 1. The scale factors of the power losses, heat transfer, gas density and load current are summarized as:

$$\begin{cases} K_{P_{\mathrm{c}}} = K_{P_{\mathrm{t}}} = K_I^2 K_l^{-2}, \\ K_{Q_{\mathrm{scc}}} = K_l^{0.6} K_{\rho_{\mathrm{f}}}^{0.4}, K_{Q_{\mathrm{tcc}}} = K_p^{0.6} K_l^{0.75}, \\ K_{Q_{\mathrm{scr}}} = K_l, K_{Q_{\mathrm{tcr}}} = K_l, \\ K_{Q_{\mathrm{ec}}} = K_l^{0.9}, K_{Q_{\mathrm{er}}} = K_l, \\ K_{\rho_{\mathrm{f}}} = K_l, \ K_t = K_l^2, \ K_I = K_l^{1.5}, \ K_p = K_l^{0.417} \end{cases} \quad (14)$$

Considering the restriction of experimental conditions and fabrication, a 1/4-scale model is feasible for the tests. As the dimensional scale factor is 4, the other scale factors are calculated as:

$$\begin{cases} K_{\rho_{\mathrm{f}}} = 4, \ K_t = 16, \ K_I = 8, \ K_p = 1.78 \\ K_h = 0.87, K_{\lambda_{\mathrm{e}}} = 4, \\ K_{Q_{\mathrm{scc}}} = K_{Q_{\mathrm{tcc}}} = K_{Q_{\mathrm{scr}}} = K_{Q_{\mathrm{tcr}}} = K_{Q_{\mathrm{er}}} = 16, \\ K_{Q_{\mathrm{ec}}} = 14 \end{cases} \quad (15)$$

In this way, the scaling relationships of convection and radiation can be fulfilled simultaneously without heat flow compensation. The criterions of Π_1-Π_{16} are fulfilled, and Π_{17} is approximately fulfilled. Dimension parameters of the full scale and the 1/4-scale GIB are compared in Table 1.

Table 1. Dimension Parameters of Full Scale and 1/4-scale GIB

	Full scale (single-phase)	Full scale (three-phase)	1/4 scale (single-phase)	1/4 scale (three-phase)
D_{ci}/mm	150	65	37.5	16.25
D_{co}/mm	180	85	45	21.25
D_{ei}/mm	470	492	117.5	123
D_{eo}/mm	500	508	125	127

3. Calculation and Validation

The structure of GIB is deemed symmetrical. In this section, in order to reduce the computation cost without the loss of accuracy, two-dimensional (2-D) finite models are employed to describe the full scale and the 1/4-scale GIB in the solution procedure, as shown in Figure 3. The FEM is applied to solve the coupled electromagnetic-fluid-thermal problem [13, 14]. Steady-state temperature rise, current density and convective heat transfer coefficient of the 1/4-scale models are compared with those of the prototypes. Simulation parameters of the prototype and the scale models are given in Table 2. The analysis presented in this paper is based on the following assumptions:

a) The GIB is infinitely long.
b) Radiation effect of the SF_6 gas is disregarded.

The density, viscosity and conductivity of the SF_6 gas and air are temperature dependent, while the specific heat is considered as constant.

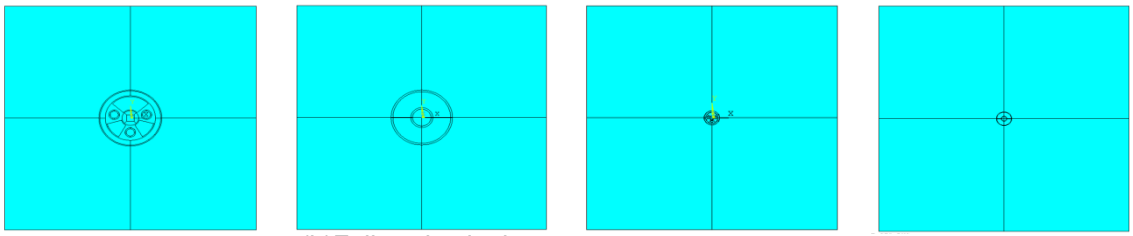

(a) Full scale three-phase (b)Full scale single-phase (c) 1/4-scale single-phase (d) 1/4-scale single-phase

Figure 3. Finite Element Models of the Full Scale and 1/4-scale GIB

Table 2. Simulation Parameters of Full Scale and 1/4-scale GIB

parameters	Full scale (single-phase)	Full scale (three-phase)	1/4 scale (single-phase)	1/4 scale (three-phase)
I/A	5000	2000	625	250
t/ms	20	20	1.25	1.25
SF_6 pressure /Mpa	0.35	0.35	0.0875	0.2
T_a/□	23	23	23	23

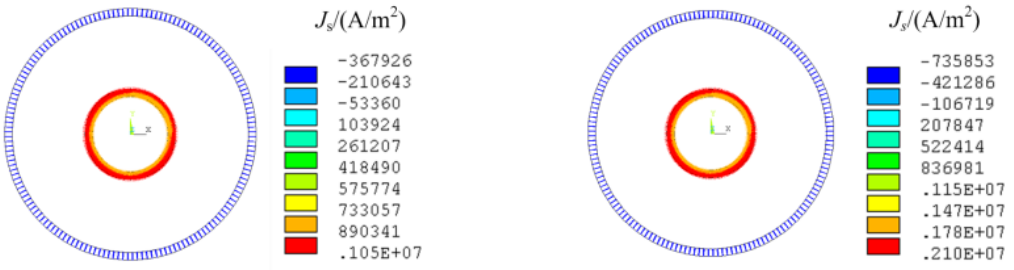

(a) Full scale single-phase bus bar (b) 1/4-scale single-phase bus bar

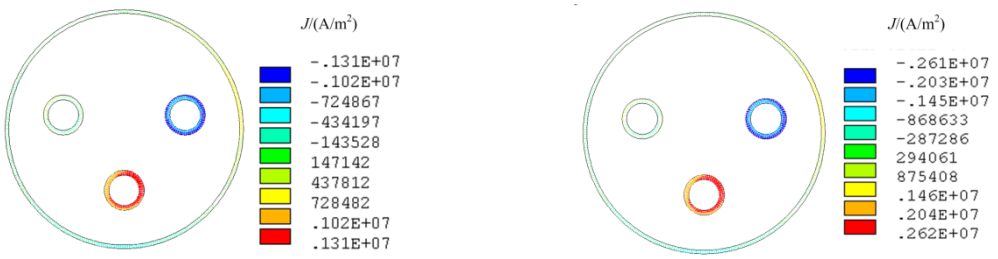

(c) Full scale three-phase bus bar (d) 1/4-scale three-phase bus bar

Figure 4. Current Density Distributions

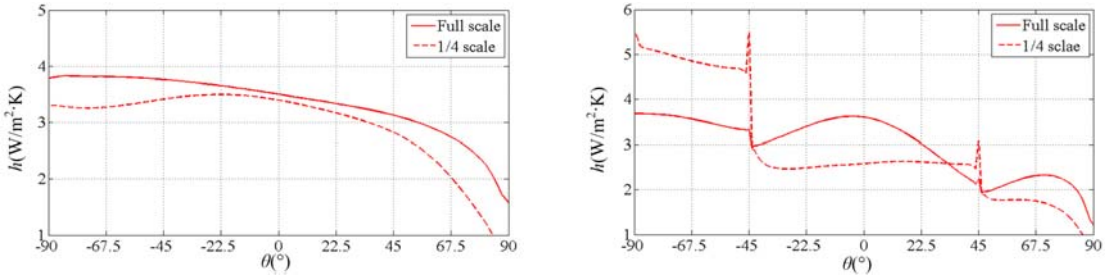

(a) Full scale single-phase bus bar (b) 1/4-scale single-phase bus bar

Figure 5. Convective Heat Transfer Coefficient on Surfaces of the GIB

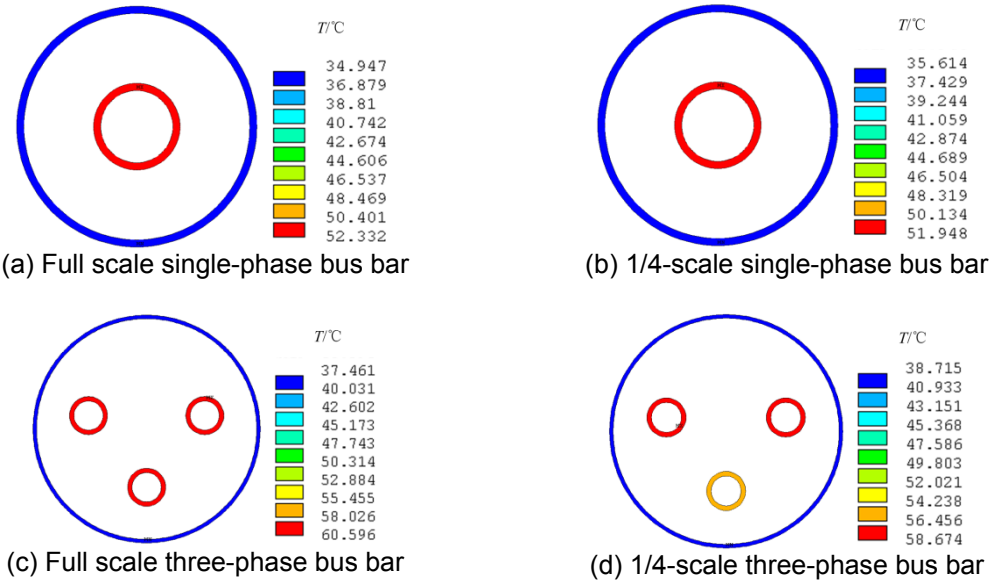

(a) Full scale single-phase bus bar (b) 1/4-scale single-phase bus bar

(c) Full scale three-phase bus bar (d) 1/4-scale three-phase bus bar

Figure 6. Temperature Distribution on Conductors and Enclosure

The current density of the scale models shares the same distributions with the prototypes, and the values of the scale models are accurately 2 times larger than those of the prototype, which demonstrates the scaling relationships of electromagnetic field, as shown in Figure 4. Comparison between convective heat transfer coefficients on the enclosure external surface of full scale and 1/4-scale GIB is shown in Figure 5. Note that the convective heat transfer coefficients of the scale models have been converted by multiplying its scale factor which is 0.87 in this paper. The converted convective heat transfer coefficient is close to but not exactly the same as those of the prototype because of the approximation made in the scaling of convection. Steady-state temperature distribution on the conductor(s) and enclosure of the prototypes and scale models are given in Figure 6. The temperature distribution of scale model corresponds well with that of prototype. Moreover, the calculated temperatures are compared with the tested temperatures of the single-phase bus bar referred in [4], as shown in Table 3. Close agreement between the calculated temperatures and the tested temperatures can be regarded as a good validation for the scaling method proposed in this paper.

Table 3. Comparison between Calculated and Tested Temperature

Method	Full scale				1/4-scale			
	I=5000 A		*I*=7000 A		*I*=625 A		*I*=875 A	
	T_c	T_e	T_c	T_e	T_c	T_e	T_c	T_e
Calculated	52.3	36.0	74.2	45.9	52.0	36.5	75.4	47.4
Tested	50	36	72	50	—	—	—	—

4. Conclusion

In order to avoid costly prototyping in the design of GIB, a scaling method is investigated to explore the electromagnetic-thermal characteristics of a full scale GIB. With regard to the scaling of power losses and heat transfer, Maxwell's equations and non-dimensional correlations are employed, respectively, to analyze the scaling relationships of power losses and heat transfer. The 1/4-scale electromagnetic-thermal finite element models of single- and three-phase GIB are designed. The correctness of the scaling methodology and the simulation calculation is validated by the close agreement between the calculated results and tested results. The scale model proposed in this paper can be used to study the electromagnetic-thermal characteristics of GIB prototype, which shows practical significance and economical benefit.

References

[1] Hedia H, Henrotte F, Meys B. Arrangement of phases and heating constraints in a busbar. *IEEE Transactions on Magnetics*. 1999; 35(3): 1274--1277.
[2] Ho SL, Li Y, Lin X. Calculations of eddy current, fluid, and thermal fields in an air insulated bus duct system. *IEEE Transactions on Magnetics*. 2007; 43(4): 1433-1436.
[3] Ho SL, Li Y, Lo EWC. Analyses of Three-Dimensional Eddy Current Field and Thermal Problems in an Isolated Phase Bus. *IEEE Transactions on Magnetics*. 2003; 39(3): 1515-1518.
[4] Minaguchi D, Ginuo M, Itaka K. Heat transfer characteristics of gas-insulated transmission lines. *IEEE Transactions on Power Delivery*. 1986; PWRD-1(1): 2-9.
[5] Chakir A, Sofiane Y, Aquelet N. Long term test of buried gas insulated transmission lines (GIL). *Applied Thermal Engineering*. 2003; 23(13): 1681-1696.
[6] Brubaker MA, Lindgren SR, Frimpong GK. Streaming electrification measurements in a 1/4-scale transformer model. *IEEE Transactions on Power Delivery*. 1999; 14(3): 978-985.
[7] He ZY, Tang GF, Li N. Study of high power electronic equipment test methodology. *Transactions of China Electrotechnical Society*. 2007; 22(1): 67-73.
[8] Shi GJ, Wang DY. Ultimate strength model experiment regarding a container ship's hull structures. *Ships and Offshore Structures*. 2012; 7(2): 165-184.
[9] Zhang YD, Ruan JJ, Wang Y. Scaling study in a capacitor-driven railgun. *IEEE Transactions on Plasma Science*. 2011; 39(1): 215-219.
[10] Shannon RL. Thermal scale modeling radiation-conduction-convection system. *Journal of spacecraft*. 1973; 10(8): 485-492.
[11] Biro O, Preis K. On the use of the magnetic vector potential in the finite element analysis of three dimensional eddy currents. *IEEE Transaction on Magnetics*. 1989; 25(4): 3145-3159.
[12] Itaka K, Akari T, Hara T. Heat transfer characteristics of gas spacer cables. *IEEE Transaction on Power Application System*. 1978; PAS-97(5): 1579-1585.
[13] Wu XW, Shu NQ, Li HT. Thermal analysis in gas insulated transmission lines using an improved finite-element model. *TELKOMNIKA Indonesian Journal of Electrical Engineering*. 2013; 11(1): 458-467.
[14] Rajagopala K, Panduranga V, Lunavath H. Computation of electric field and thermal properties of 3-phase cable. *TELKOMNIKA Indonesian Journal of Electrical Engineering*. 2012; 10(2): 265-274.